Electronic Supplementary Material (ESI) for Journal of Materials Chemistry A

Electronic Supplementary Information

Monocrystalline VO_2 (B) nanobelts: large-scale synthesis, intrinsic peroxidase-like activity and application in biosensing

Guangdi Nie,[a] Liang Zhang,[b] Junyu Lei,[a] Liu Yang,[a] Zhen Zhang,[a] Xiaofeng Lu*[a] and Ce Wang*[a]

[a] *Alan G. MacDiarmid Institute, Jilin University, Changchun, 130012, P. R. China. Fax-Tel: +86-431-85168292; E-mail: xflu@jlu.edu.cn; cwang@jlu.edu.cn*

[b] *Department of Polymer Science and Engineering, University of Science and Technology Beijing, Beijing, 100083, P. R. China.*

Experimental

Materials

Hydrogen peroxide (H_2O_2, 30%, Beijing Chemical Works) and Glucose oxidase (GOx, 100-250 $U \cdot mg^{-1}$, BR, Shanghai Kayon Biological Technology Co. Ltd) were stored in a refrigerator at -20°C. Other chemical reagents including vanadyl acetylacetonate ($VO(acac)_2$, 95%), concentrated hydrochloric acid (HCl, AR), 3,3',5,5'-tetramethylbenzidine (TMB, BR), sodium hydroxide (NaOH, AR), acetic acid (HAc, AR), dopamine hydrochloride (DA, 98%), L-ascorbic acid (AA, AR), citric acid (CA, 99+%) and so forth were used as received without any further purification. Ultrapure water was utilized for the preparation of all aqueous solutions.

Synthesis of catalysts

VO_2 (B) nanobelts were fabricated as follows: a certain amount of $VO(acac)_2$ (2.5mmol) was dissolved in 30 mL of distilled water containing 0.08 M HCl under magnetic stirring to form a clear and transparent solution, which was then transferred into a 40 mL Teflon-lined autoclave. The reaction proceeded in an electric oven at 160°C for 24 h. After cooling down, the final blue-black product was collected by centrifugation, washed thoroughly with distilled water and ethanol, and ultimately dried at 40°C for characterization and further use.

Apparatus

The morphology of the sample was observed by a cold field-emission scanning electron microscopy (FESEM, Hitachi SU8020) and a transmission electron microscopy (TEM, JEOL JEM-1200 EX) operated at 3.0 and 100 kV, respectively. High-resolution TEM (HRTEM) images, selected area electron diffraction (SAED) patterns and energy dispersive X-ray (EDX) analysis were conducted on a FEI Tecnai G2 F20) electron microscope at an acceleration voltage of 200 kV. X-Ray diffraction (XRD, PAN-alytical B.V. Empyrean) with CuKα radiation was employed to investigate the crystallographic structure of the as-prepared product. Fourier-transform infrared (FTIR) spectra of KBr powder-pressed pellets were recorded on a Bruker Vector 22 Spectrometer. The chemical composition of the resulting VO_2 (B) nanobelts was characterized by X-ray photoelectron spectroscopy (XPS, Thermo Scientific ESCALAB250). The peroxidase-like catalytic activity was measured by ultra-violet-visible (UV-vis) spectra performed on Shimadzu UV-2501 PC spectrometer.

Colorimetric assay

In a typical colorimetric experiment, unless otherwise stated, 10 μL of catalyst aqueous dispersion (3 $mg \cdot mL^{-1}$) was added to 3 mL of acetate buffer solution (0.1 M, pH = 5.0) consisting of 100 μM TMB and 5 mM H_2O_2. Afterwards the sample in cuvette was positioned immediately in the cell holder of UV-Vis spectrophotometer for the steady-state kinetic measurements which were implemented in time course mode by monitoring the absorbance changes at 650 nm. The apparent kinetic parameters in the Michaelis-Menten equation were calculated on the basis of Lineweaver-Burk plot: $1/v = K_m/V_{max} \cdot (1/[S] + 1/K_m)$, where v, K_m, V_{max} and $[S]$ represent, respectively, the initial velocity, the Michaelis constant, the maximal reaction velocity and the substrate concentration. DA, AA and CA with the same content of 5 mM were used instead of H_2O_2 for comparison purpose to verify the selectivity of VO_2 (B) nanobelts.

As for the determination of glucose, there is really no essential difference from the mentioned conditions except for that 10 μL of 10 mg·mL^{-1} GOx and 100 μL of glucose with different concentrations in 500 μL of phosphate buffer solution (10 mM, pH = 7.0) should be incubated at 37 °C for 30 min before approximately 3 mL of mixed specimen was prepared, and that absorption spectra were tracked at the time of 120 s to survey the oxidation reaction of the substrate TMB.

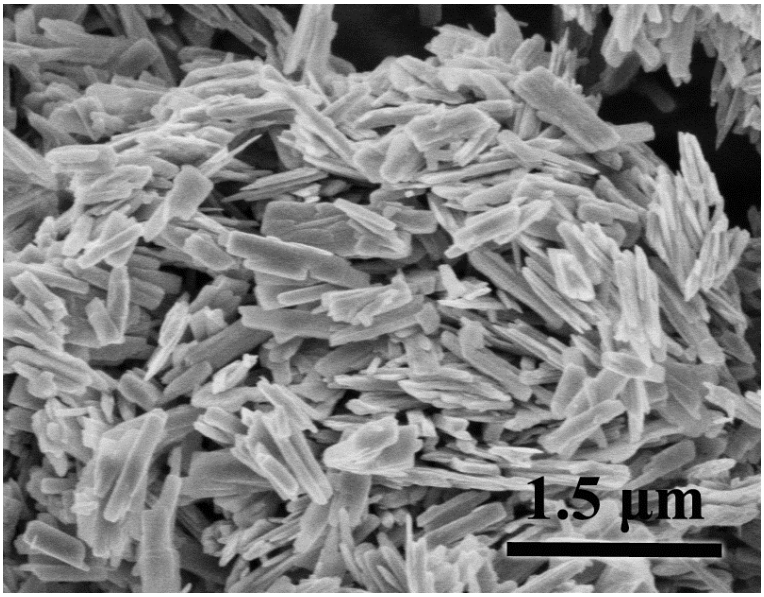

Fig. S1 SEM image of the belt-like VO_2 (B) nanostructures.

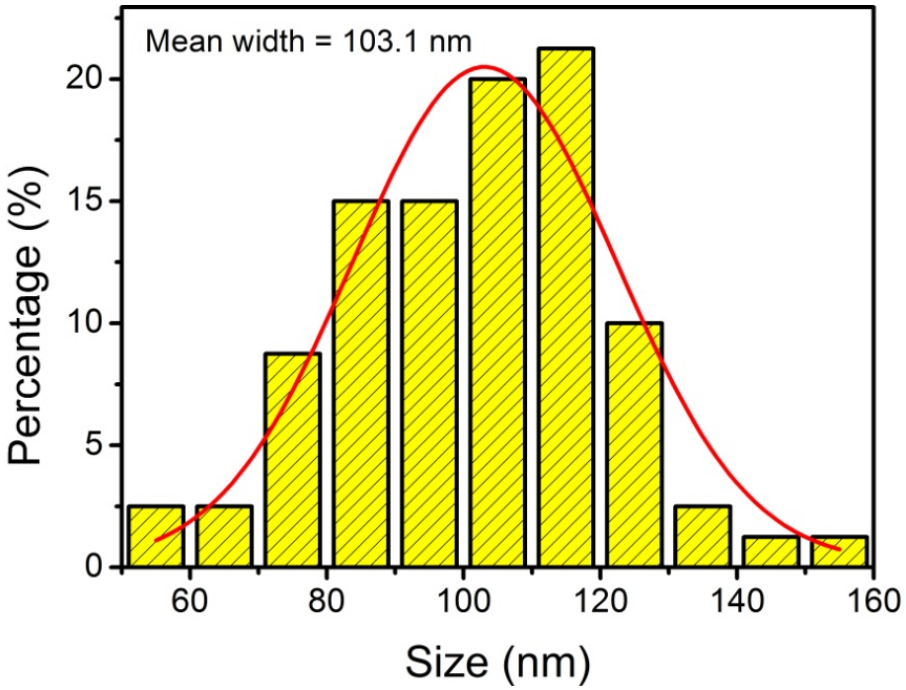

Fig. S2 Width distribution of VO_2 (B) nanobelts counted from the TEM image.

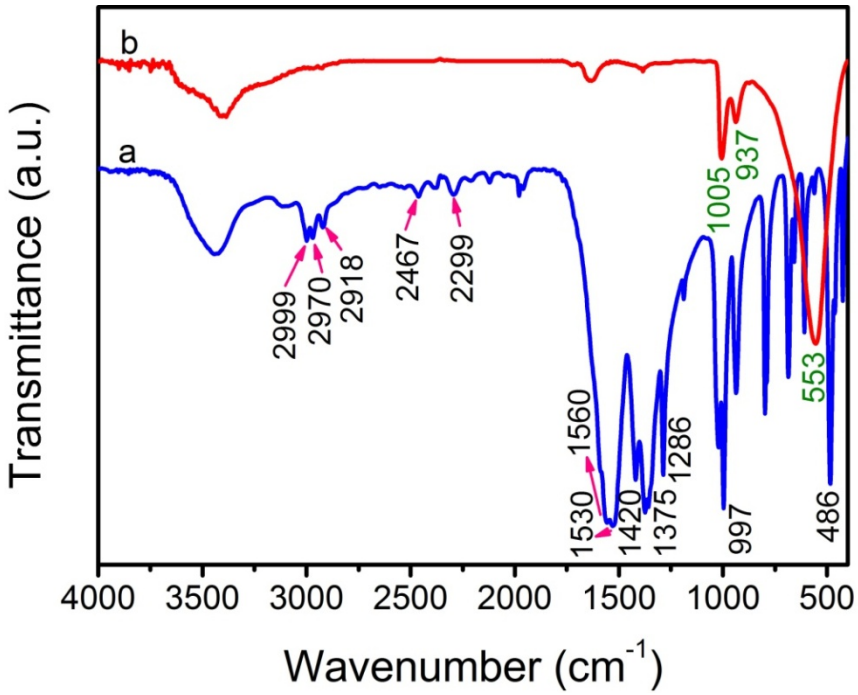

Fig. S3 FTIR spectra of (a) $VO(acac)_2$ raw materials and (b) VO_2 (B) nanobelts.

As depicted in Fig. S3a, the FTIR spectrum of $VO(acac)_2$, which is in perfect agreement with the reference,[1] the weak and overlapping bands in the region of 2900~3000 cm^{-1} are aroused by the symmetric and antisymmetric vibrations of CH_3. The stretching vibrations of -CO-CH-CO- are observed at 2467 and 2299 cm^{-1}. The peaks positioned at 1560, 1530 and 1375 are ascribed to C=O vibration modes. The stretching vibrations of C-O and C=C appear separately at 1420 and 1286 cm^{-1}. Moreover, the characteristic peaks at 997 and 486 cm^{-1} indicate the existence of V=O and V-O bonds. With regard to the as-prepared VO_2 (B) nanobelts, by contrast, no peaks belong to $VO(acac)_2$ are discovered in Fig. S3b, suggesting the complete hydrolysis of the precursor. In the light of the earlier report,[2] the bands at 553, 937 and 1005 cm^{-1} can be identified to be intrinsic for VO_2 (B), which are attributed to the V-O-V octahedral bending deformation modes, the coupled vibration of V=O and V-O-V as well as the stretching of short V=O, respectively.

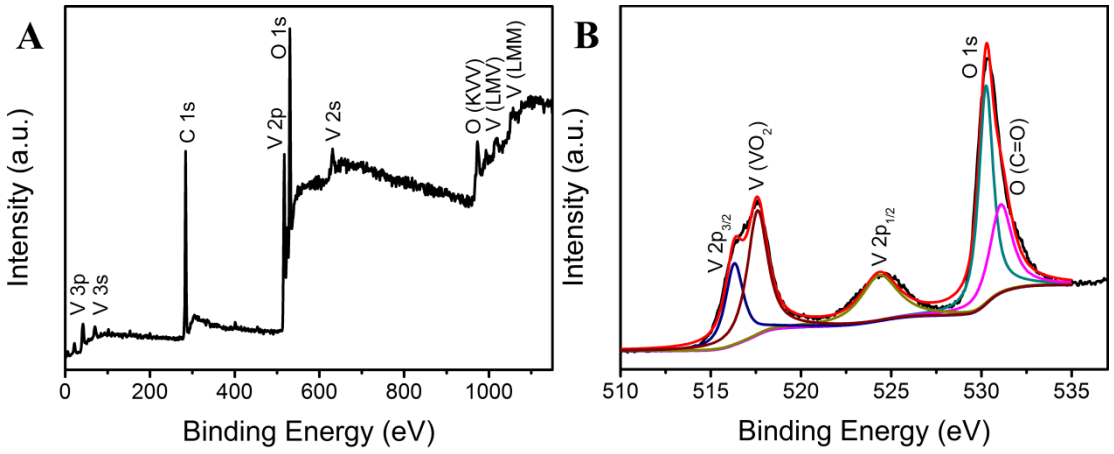

Fig. S4 XPS spectra of VO_2 (B) nanobelts: (A) full survey spectrum, (B) V 2p and O 1s regions.

In order to study the surface electronic state and chemical composition of the final products, their XPS spectra were given in Fig. S4. The wide-scan XPS spectrum (Fig. S4A) distinctly reveals the presence of V, C and O elements, among which the signal of C should primarily be imputed to the absorbed carbon dioxide. To deeply evaluate the binding property of the elements in VO_2 (B), high-resolution XPS spectrum (Fig. S4B) can be fitted with three main peaks centered at 516.3, 517.6 and 524.3 eV for V 2p region, which are associated severally with V $2p_{3/2}$, VO_2 and V $2p_{1/2}$,[3,4] expounding that V (Ⅳ) as the exclusive valence state exists in the final nanobelts, and another predominant peak accompanied by carbonyl (C=O) line for O 1s region.

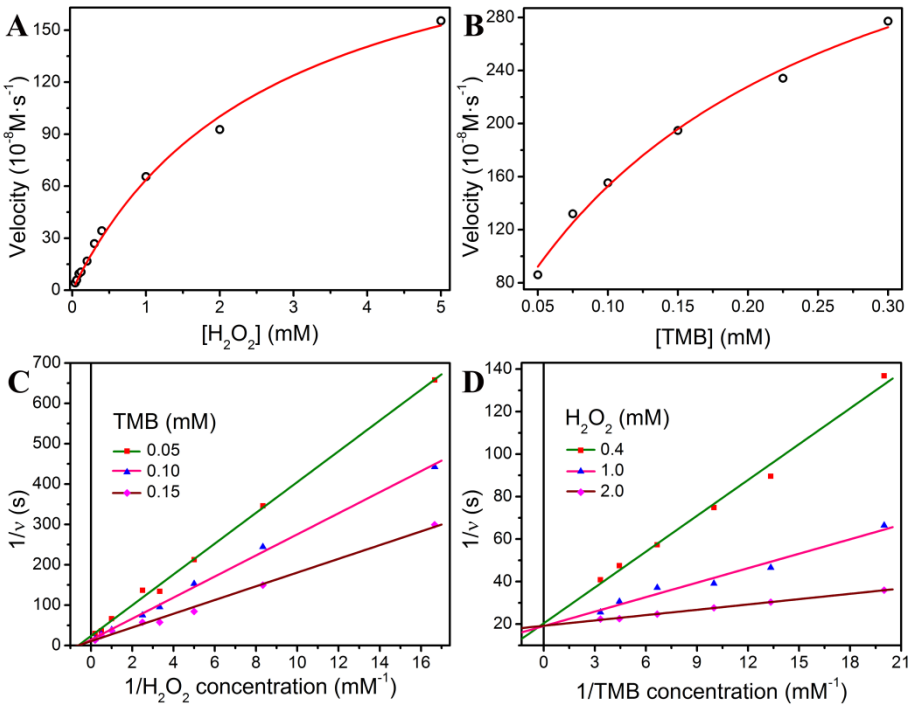

Fig. S5 Steady-state kinetic assay of VO_2 (B) nanobelts. The catalyst concentration was fixed at 10 μg·mL^{-1} in 3 mL of acetate buffer solution (0.1 M, pH = 5.0). (A) TMB concentration was kept constant at 100 μM and the H_2O_2 concentration was varied. (B) H_2O_2 concentration was maintained at 5 mM and the TMB concentration was varied. Double reciprocal plots of VO_2 (B) catalytic activity for the two substrates (C) H_2O_2 and (D) TMB. Details were described in the Experimental section.

Table S1 Comparison of the kinetic parameters between different nanomaterials and horseradish peroxidase (HRP) with (A) H_2O_2 and (B) TMB as the substrates.

A	Catalyst	K_m [mM]	V_{max} [10^{-8}M·s^{-1}]
Substrate H_2O_2	HRP[5]	3.7	8.71
	Fe_3O_4 MNPs[5]	154	9.78
	$ZnFe_2O_4$ MNPs[6]	1.66	7.74
	Co_3O_4 GNs[7]	245	28.5
	PB/γ-Fe_2O_3 MNPs[8]	323.6	117
	VO_2 (B)	1.69	177

B	Catalyst	K_m [mM]	V_{max} [10^{-8}M·s^{-1}]
Substrate TMB	HRP[5]	0.434	10.0
	Fe_3O_4 MNPs[5]	0.098	3.44
	$ZnFe_2O_4$ MNPs[6]	0.85	13.31
	Co_3O_4 GNs[7]	0.12	33.2
	PB/γ-Fe_2O_3 MNPs[8]	0.307	106
	VO_2 (B)	0.146	131

Table S2 Reproducibility between two batches of VO_2 (B) nanobelts prepared at different times using the same method.

Batch No.	1	2	RSD (%)
Catalytic activity (%)	100±5.5[a]	94.5±5.0[a]	5.9

[a] RSD for nine repeated measurements.

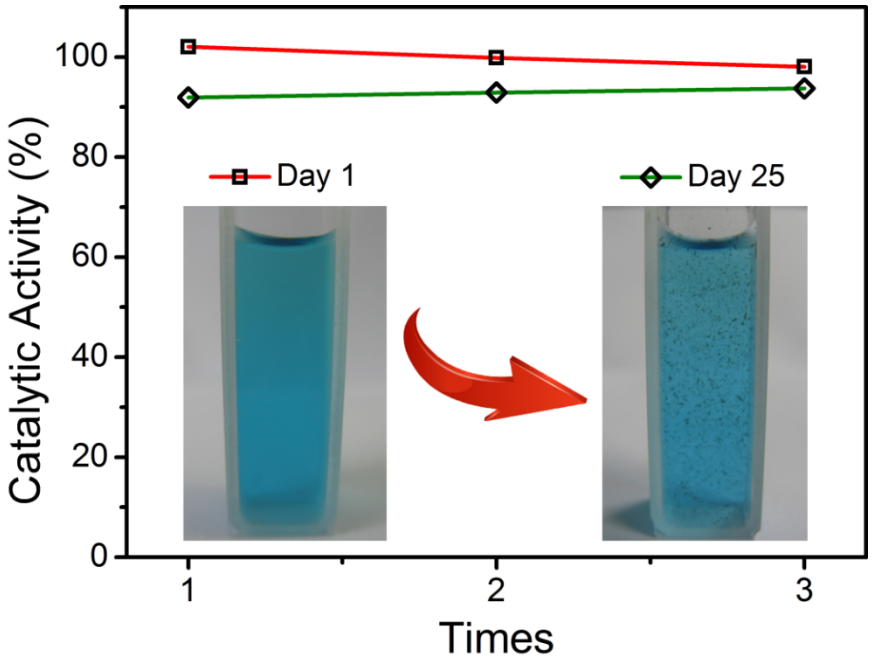

Fig. S6 Long-term stability of VO_2 (B) stock solution with three duplicate determinations. Inset:

the corresponding pictures of colored products.

References

1 L. J. Mao, C. Y. Liu and J. Li, J. Mater. Chem., 2008, **18**, 1640-1643.
2 S. R. Popuri, M. Miclau, A. Artemenko, C. Labrugere, A. Villesuzanne and M. Pollet, Inorg. Chem., 2013, **52**, 4780-4785.
3 Y. Xu, L. Zheng and Y. Xie, Dalton Trans., 2010, **39**, 10729-10738.
4 X. Y. Chen, X. Wang, Z. H. Wang, J. X. Wan, J. W. Liu and Y. T. Qian, Nanotechnology, 2004, **15**, 1685-1687.
5 L. Z. Gao, J. Zhuang, L. Nie, J. B. Zhang, Y. Zhang, N. Gu, T. H. Wang, J. Feng, D. L. Yang, S. Perrett and X. Y. Yan, Nat. Nanotechnol., 2007, **2**, 577-583.
6 L. Su, J. Feng, X. M. Zhou, C. L. Ren, H. H. Li and X. G. Chen, Anal. Chem., 2012, **84**, 5753-5758.
7 J. F. Yin, H. Q. Cao and Y. X. Lu, J. Mater. Chem., 2012, **22**, 527-534.
8 X. Q. Zhang, S. W. Gong, Y. Zhang, T. Yang, C. Y. Wang and N. Gu, J. Mater. Chem., 2010, **20**, 5110-5116.
9 W. W. He, Y. Liu, J. S. Yuan, J. J. Yin, X. C. Wu, X. N. Hu, K. Zhang, J. B. Liu, C. Y. Chen, Y. L. Ji and Y. T. Guo, Biomaterials, 2011, **32**, 1139-1147.